

Comparative Studies of MgB₂/Mg Nano-Composites and Press-Sintered MgB₂ Pellets

Qiang Li, L. Wu, Y. Zhu, A. R. Moodenbaugh, G. D. Gu, M. Suenaga, Z. X. Ye, and D. A. Fischer

Abstract—We present our studies of superconducting and microstructural properties of bulk MgB₂/Mg nano-composites and press-sintered MgB₂. TEM investigation revealed that the composites are very dense, consisting of nano-sized MgB₂ grains connected by the well-defined clean grain boundaries (GB). Both amorphous and structural intact GB's were observed in the press-sintered samples. Magnetization and transport measurements showed that the composite carried over 1 MA/cm² critical current density (J_c) at 5 K and self-field, while the pressed sintered MgB₂ has $J_c \sim 0.25$ MA/cm² at 5 K and self-field. The origin of substantially higher J_c found in the composites is mostly due to their nano-sized grains and clean grain boundaries.

Index Terms—Critical current, grain boundary, MgB₂ superconductors, nano-composites.

I. INTRODUCTION

THE discovery of binary MgB₂ superconductor [1] has generated great interest in the practical applications of superconductors, owing to the abundance of Mg and B, as well as much simpler crystalline structures of MgB₂ compared to high T_c cuprates. Soon afterwards, both MgB₂ thin film [2], [3] and wires [4] with high J_c were successfully fabricated with rather conventional processing methods. At the present time, there are several unsettled practical issues related to the power application of MgB₂. Three of the most noticeable ones are: 1) relatively low H_{c2} and moderate flux pinning strength; 2) brittle due to the inherited hexagonal lattice structure; 3) flux jumps in high J_c bulk MgB₂ at low temperatures [4]. The origin of flux jump is related to the thermo-magnetic instability of the motion of magnetic vortices in a type II superconductor. It is well known that flux jump can result in a large-scale flux avalanche in the critical state, which could have a devastating consequence in such practical applications as energy storage and power transmission. For practical applications, one has to develop a method to increase the flux pinning in the bulk MgB₂, while improving the mechanical performance, as well as stabilizing the critical states to prevent flux avalanche. To address those practical issues, we developed a process of producing high density MgB₂/Mg nano-composites with J_c over 1 MA/cm² at 4.2 K and self-field [5]. In this work, we present our comparative studies of superconducting and microstructural properties of this composite



Fig. 1. A chunk of MgB₂/Mg nano-composite cut and shaped into 8 mm diameter and 1 mm thick disk.

and bulk pressed-sintered MgB₂. Our studies showed that the grain-size and clean grain boundaries played an important role in the critical current carrying capability of bulk polycrystalline MgB₂ materials. Furthermore, addition of pure Mg improves the ductility of the material, as well as stabilizing the flux motion in the critical states.

II. EXPERIMENTAL DETAILS

MgB₂/Mg nano-composites were prepared using 99.99% Mg ingot and 99.99% B powder placed into a 450 mm long alumina crucible. The assembly was heated in a temperature gradient 600–1200 °C, then furnace cooled [5]. Fig. 1 shows a chunk of this composite cut and shaped into 8 mm diameter and 1 mm thick disk. After light polishing, the composite exhibits a shining metallic gray surface, as shown in Fig. 1. It was found that the composites were much less brittle as compared to the pressed sintered polycrystalline MgB₂ pellets.

For comparison, we also prepared monolithic samples using commercial MgB₂. The powder was pressed into a pellet, sealed into an alumina tube, and sintered under Mg vapor, ~ 300 torr, at 1050 °C for 24 hours, followed by furnace cooling. The resulting Mg-rich pellets looked gray. Cut and polished specimens were examined using an optical microscope. They appeared shiny and dense ($\sim 95\%$ of theoretical density) with averaged MgB₂ grain size ~ 10 μ m.

In addition to the standard material characterization techniques, we used several advanced structural and phase characterization facilities at BNL. Among them are the soft x-ray absorption spectroscopy (XAS) and the advanced high resolution TEM with nanobeam electron energy loss spectroscopy (EELS). The MgB₂ boron K -edge XAS were performed at the beam line U7A at the BNL National Synchrotron Light Source with an *in situ* mechanical polishing apparatus in 3×10^{-8} torr vacuum chamber. Microstructural and structural defects were

Manuscript received on August 5, 2002. This work was supported by the U. S. Department of Energy, under Contract DE-AC02-98CH10886.

Q. Li, L. Wu, Y. Zhu, A. R. Moodenbaugh, G. D. Gu, M. Suenaga, and Z. X. Ye are with Brookhaven National Laboratory, Upton, NY 11973-5000 USA (e-mail: qiangli@bnl.gov).

D. A. Fischer is with Materials Science and Engineering, National Institute of Standards and Technology, Gaithersburg, MD 20899 USA.

Digital Object Identifier 10.1109/TASC.2003.812070

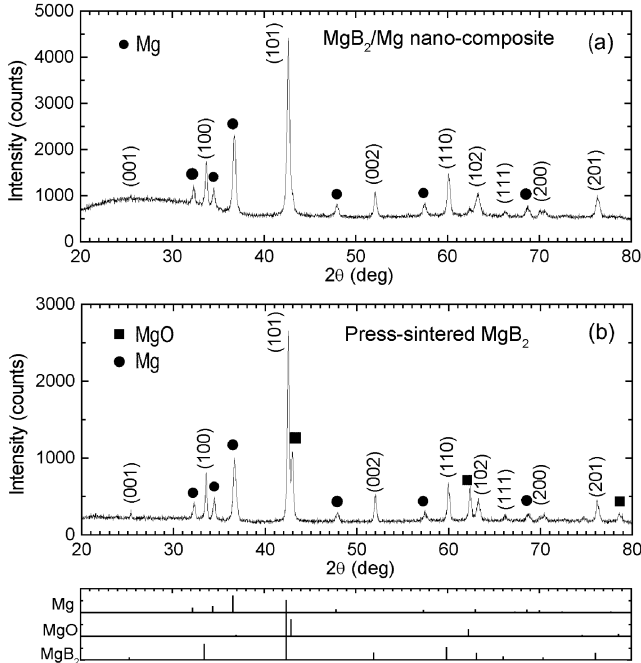


Fig. 2. X-ray diffraction measurements of MgB_2/Mg nano-composite (a) and press-sintered MgB_2 pellet (b). The diffraction peaks are indexed to MgB_2 , and peak positions of all three phases (MgB_2 , Mg, and MgO) are marked in the lower panel.

characterized using a JEOL3000F electron microscope with a field emission source operated at 300 kV.

For superconducting properties, bulk magnetization measurements were performed in the Quantum Design's SQUID magnetometer using a bulk slab cut from the composites or the pressed-sintered pellet with the magnetic field applied along the longest dimension of the slab. Direct dc transport measurements using standard four-probe configuration were performed at an exchange gas cooled cryostat equipped with 9 T superconducting magnet. The transport measurements were only performed at relative high temperatures, or at low temperatures and high field to avoid the sample heating, when J_c of the specimen are not too high.

To study the grain connectivity, we also used the magneto-optical (MO) apparatus similar to that used by Polyanski, *et al.* [6]. For nano-composites, the grain size is below the resolution limit of MO technique ($\sim 2 \mu\text{m}$). Flux penetration to individual grains can not be directly imaged. However, electromagnetic granularity of a bulk specimen can be determined from the global MO images taken on the magnetic shielding state to conclude whether the grain boundaries are strongly or weakly coupled at the applied external field.

III. RESULTS AND DISCUSSIONS

A. X-Ray Diffraction Measurements

X-ray powder diffraction was used to identify the bulk phase, approximate composition, and lattice parameters. Diffraction patterns were obtained with $\text{Cu K}\alpha$ radiation (wavelength $\lambda =$

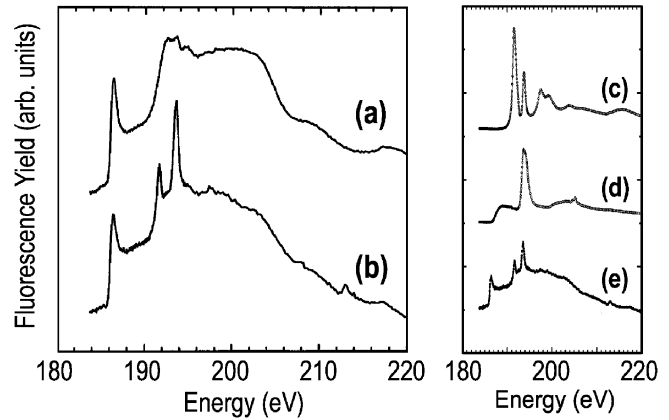


Fig. 3. XAS spectra of the K edge of boron in MgB_2 with *in situ* cleaned (a) and uncleaned (b) surface of the MgB_2/Mg nano-composites. For comparison, boron nitride (c), boron oxide (d), and powder MgB_2 are shown in the left panel.

0.154178 nm) over a range of $10^\circ < 2\theta < 100^\circ$ using 0.02° steps. Fig. 2 shows the x-ray diffraction pattern of a powder ground from the nano-composites (a) and the press-sintered pellets (b). The diffraction peaks are indexed to MgB_2 , and peak positions of all three phases (MgB_2 , MgO, and Mg) are marked in the lower panel.

Detailed studies showed that the MgB_2/Mg nano-composite consists of $\sim 75\%$ MgB_2 and 25% metal Mg. The tiny trace of MgO is believed to be the result of oxidized Mg during the powdering, which was confirmed by the *in situ* XAS measurements (will be discussed in the next section). For the pressed-sintered pellet, the majority $\sim 70\%$ is MgB_2 , while the remainder is comprised of MgO periclase and metal Mg.

B. XAS Spectra of the K Edge of Boron in MgB_2

The MgB_2 boron K-edge XAS studies are found very helpful to identify the boron-based compounds in MgB_2 . We note that MgB_2 , once exposed to air, forms a boron-containing impurity surface layer. The surface impurities could significantly complicate the analysis of the true bulk phase and composition by standard techniques, such as diffraction and the energy dispersion spectrum (EDS) in the electron microscope.

In order to obtain a fresh surface of the MgB_2/Mg composites, a mechanical polishing apparatus was installed in the 3×10^{-8} torr vacuum chamber. We found that the boron-containing impurity surface layer gives rise to extra peaks at 191.7 and 193.6 eV in the boron XAS spectrum, as shown in Fig. 3(b). The XAS spectrum of an *in situ* cleaned sample of the MgB_2/Mg composites is shown in Fig. 3(a), which exhibits only one sharp peak at 186.5 eV and two broad maxima at ~ 195 and ~ 200 eV. The sharp peak at 186.5 eV is the characteristic peak of MgB_2 [7]. Also shown in the left panel of Fig. 3 are XAS spectra of boron nitride (c), boron oxide (d), and powdered MgB_2 (e). For an *in situ* cleaned sample of the press-sintered MgB_2 pellets, we found that the XAS spectrum was similar to that shown in Fig. 1(b), which indicates that boron-containing impurities are presented in the bulk of the press-sintered pellets.

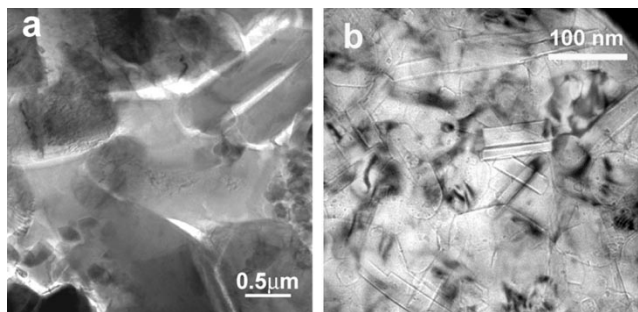


Fig. 4. TEM images of the press-sintered MgB₂ pellet (a) and the MgB₂/Mg nano-composite (b).

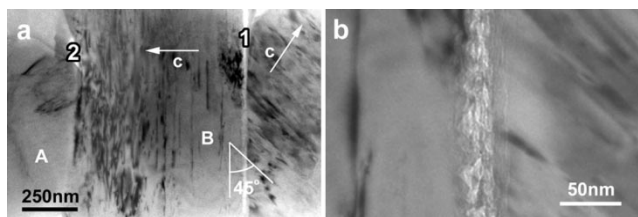


Fig. 5. (a) Three grains with two typical grain boundaries (GB's) in the press-sintered MgB₂ pellet. 1: amorphous GB, and 2: structurally intact GB. (b) Enlargement of the amorphous GB.

C. Grain Morphology of the Press-Sintered MgB₂ Pellets and the MgB₂/Mg Nano-Composites

Fig. 4 is the TEM images showing the grain morphology of the press-sintered MgB₂ pellets (a) and the MgB₂/Mg nano-composites (b). MgB₂ crystals and MgO second phase particles were found in both samples. No other phases, such as MgB₄ and MgB₇ were detected. Metal-magnesium-metal was not observed in the TEM samples. Highly active metal Mg in the TEM thin area was probably oxidized during the ion-milling and plasma-cleaning process prior to the TEM imaging. For the press-sintered MgB₂ samples, the individual MgB₂ grains, in general, seemed rather clean and dense [8]. However, because of the existence of the aggregates of solidified MgO and many poorly sintered, and poorly connected grains, overall samples were mechanically weak. The average grain size is $\sim 10 \mu\text{m}$. For the MgB₂/Mg nano-composites, the grains are platelet shape with an averaged size of $100 \times 70 \times 20 \text{ nm}^3$. We found that the grains are packed extremely dense with all clean grain boundaries. No porosity was observed in the composites.

D. MgB₂ Grain Boundaries

There are two types of grain boundaries (GB) in the press-sintered samples. One represents poorly coupled grains with amorphous materials at the boundaries, while the other type involves well-coupled grain with structurally intact boundaries. In the composites, only the later type was found with clean and well-defined boundary interfaces. Fig. 5(a) shows three grains connected by these two typical GB's in the press-sintered samples, marked as 1 and 2 for the amorphous and the intact GB's respectively. An enlarged TEM image of the amorphous GB 1 was shown in Fig. 5(b). In general, the thickness of the amorphous layer at such GB ranges from 10 to 50 nm.

Fig. 6 is the TEM images showing an example of those structurally intact GB's. Fig. 6(a) displays a two-beam image of the

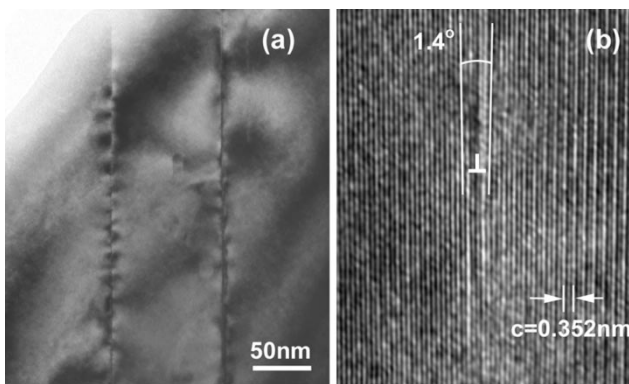


Fig. 6. A 4.1° small-angle (001) grain boundary in the press-sintered MgB₂ pellet. (a) Diffraction contrast associated with interfacial dislocations. (b) high resolution TEM image showing the alternating Mg-B layers (the (002) lattice fringes) and the 1.4° tilt component.

boundary showing the diffraction contrast of the quasiperiodic dislocation array at the interface of a 4.1° small angle (001) GB. Fig. 6(b) is a high-resolution (002) lattice image showing alternating Mg-B layers. The major component of this GB is 3.7° twist GB about the [001] axis, while the minor component is a small angle tilt.

For both the MgB₂/Mg composite and the pressed-sintered samples, The majority GB's are (001) twist, both large-angle and small-angle, with an in-plane rotation about the *c*-axis across the interface, similar to the majority GB's in Bi₂Sr₂CaCu₂O₈ (Bi2212) superconductors [9]–[11]. This can be attributed to the layered nature of the MgB₂ crystalline structure.

E. Nano-Probe EELS Study of MgB₂ Grain Boundaries

The fine structure of the boron *K* pre-edge was also studied using high-resolution nano-probe EELS for large-angle structurally intact grain boundaries. It has been shown that the changes in the near edge structure observed in EELS is directly related to the change of the empty boron *p* states near the Fermi level [7].

Fig. 7 is an example revealing the difference between the fine structure of the boron *K*-edge acquired at the grain boundary (GB) and at the grain interior (GI, 50 nm away from the GB) for the press-sintered MgB₂ samples. Note the change of the core-loss intensity of the pre-peak marked by the vertical thin lines in the spectra. The dashed lines represent the spectra after plural scattering removal. We observed the shoulder at the onset of the edge of the bulk spectrum (GI) associated with the empty *p_xp_y* states. This shoulder is lacking in the grain boundary spectrum (GB). Electron diffraction and high-resolution imaging analysis show that the grain interface is a 20° (001) tilt boundary with densely spaced interfacial dislocations (0.9–1 nm in periodicity). At present time, it is generally recognized that the boron *p_xp_y* states are responsible for the superconductivity in MgB₂. These observations suggest that the lack of the *p_xp_y* peak at the *K*-edge of the boron in MgB₂ at the GB is the indication of hole depletion at the GB. However, the boundary width is about 1–2 nm, which is much narrower than the superconducting coherence length of MgB₂. Hence, the high angle grain boundaries probably are not a

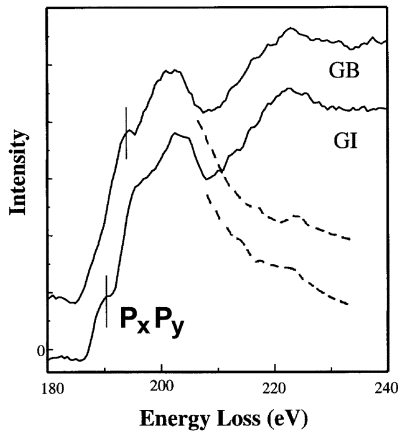


Fig. 7. Nano-probe EELS showing the fine structure of the boron K-edge acquired from a grain boundary (GB) and grain interior (GI, 50 nm away from the GB). Note the change of the core-loss intensity of the pre-peak marked by the vertical thin lines in the spectra. The dashed lines represent the spectra after plural scattering removal.

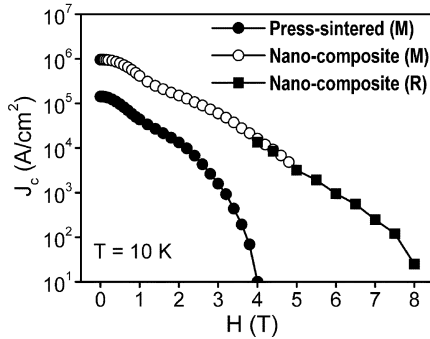


Fig. 8. Magnetic field dependence J_c of the MgB_2/Mg nano-composites and the press-sintered MgB_2 pellets at 10 K, obtained by the magnetization (M) and resistive measurements (R).

strong limiting factor for the critical current carrying capability of bulk polycrystalline MgB_2 , which is the case for most of high T_c superconductors.

F. J_c of the Press-Sintered MgB_2 Pellets and the MgB_2/Mg Nano-Composites

Based on the measurement of magnetic shielding (zero-field-cool) and Meissner effect (field-cool) at an external field of 2 Oe, both the composites and the pressed-sintered samples show sharp superconducting transitions ($T_c = 38.3$ K and 37.2 K for the composites and the pressed-sintered ones, respectively.) However, the resistive measurements using the standard four-probe configuration show higher T_c ($= 39.1$ K and 38.5 K for the composites and the pressed-sintered ones, respectively.). The difference is likely due to the proximity effect between Mg and MgB_2 .

Fig. 8 shows the magnetic field dependence of critical current density J_c of the press-sintered MgB_2 pellet and the MgB_2/Mg nano-composites at 10 K, obtained by the magnetization (M) and resistive (R) measurements. The magnetically determined J_c was obtained by applying the standard Bean critical state model to the measured magnetic hysteresis of the specimen at applied external field up to 5 T, where the entire cross section of

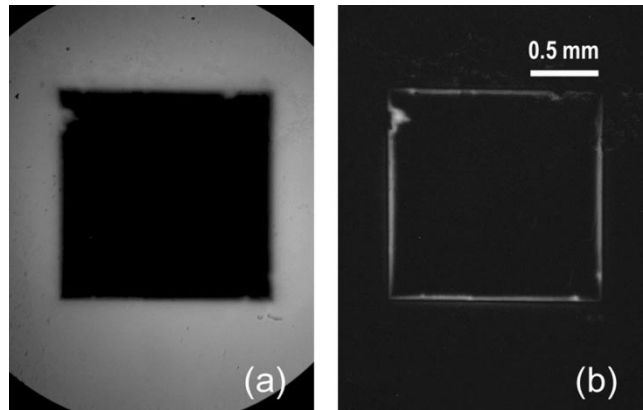


Fig. 9. MO images of the same cross-section of a square disk of the MgB_2/Mg nano-composites at 4.2 K. (a) Flux screening at maximum field of 1100 Oe, applied to the zero-field-cooled samples. (b) Remnant state showing surface pinning. Similar patterns were observed at temperatures from 4.2 K to 25 K.

the sample perpendicular to field was used in calculations. For nano-composites, we found that the J_c values determined magnetically (open circles in Fig. 8) were in excellent agreement with those measured by direct resistive method (solid squares in Fig. 8) at high fields. It is apparent that the measured critical current of the nano-composites in the critical state is indeed circulating the entire specimen. We found that the bulk J_c of the nano-composites (1.1×10^6 A/cm² at 5 K, self-field) is over four times that of the press-sintered pellet (2.5×10^5 A/cm² at 5 K, self-field).

G. MO Studies of the MgB_2/Mg Nano-Composites

To further investigate the electromagnetic granularity of our MgB_2/Mg nano-composites, we performed MO studies at maximum field of 1100 Oe. It is expected that $\sim 25\%$ addition of Mg in the MgB_2 matrix will substantially help the heat dissipation generated by the vortex motion, and thus prevent the critical state avalanche.

Fig. 9 shows the MO images of the same area of a square-disk-shaped specimen cut from the bulk MgB_2/Mg nano-composites without polishing. The broad section ($1.5 \text{ mm} \times 1.5 \text{ mm}$) of specimen was used for imaging. The cutting by the diamond saw introduced rough edges into the specimen, which was considered during the image analysis. Fig. 9(a) is the image taken at 4.2 K and at the maximum field of 1100 Oe applied to the zero-field-cooled samples. We found that external field are completely screened outside the samples. Fig. 9(b) is the remnant state after the external field was decreased from 1100 Oe to zero. Brightness intensity analysis of the MO image indicated that there is no penetration or trapping of magnetic field inside the specimen. Instead, only surface pinning of magnetic flux was observed. Similar MO images were obtained at $4.2 \text{ K} \leq T \leq 25 \text{ K}$. The MO studies further confirmed that the grain boundaries in the nano-composites are indeed strongly coupled at $4.2 \text{ K} \leq T \leq 25 \text{ K}$ and $H \leq 0.11$. In contrast, significant superconducting inhomogeneities (or granularity) were reported in the MO studies of earlier MgB_2 polycrystalline samples by Larbalestier and co-workers [12]. Up to 0.11 T, no evidence of flux jumps in our nano-composites was observed.

IV. CONCLUSIONS

In conclusion, we presented our comparative studies of superconducting and microstructural properties of the bulk MgB₂/Mg nano-composites and the press-sintered MgB₂, in order to reveal the controlling factors for the critical current of MgB₂ superconductors. We found that the nano-composites are extremely dense and carries more than four times J_c , as compared to the press-sintered pellet. Based on detailed structural and phase characterizations by TEM and XAS, we attribute the robust performance of the nano-composites to the following features found only in the nano-composite: 1) Absence of impurity segregated phases such as MgO, boron nitride, and boron oxides, which tend to act like barriers to the flow of critical current. 2) Nano-sized grains densely packed with clean grain boundaries. Since the superconducting coherence length of MgB₂ is significantly higher than the grain boundary width, the high angle grain boundaries do not likely limit the critical current of MgB₂, in opposite to the case of high T_c cuprates. MO images taken at both magnetic field shielding and the remnant state up to 1100 Oe suggest that the grain boundaries in this composite are strongly coupled. It is quite likely that these grain boundaries actually work as pinning centers. 3) Addition of Mg into the composites increases the mechanical performance. In more detained MO studies of the critical state of this composite, we observed a regular flux distribution, in consistent with the prediction of a uniform critical state model. No flux jump was observed at temperature as low as 4.2 K under maximum external field of 0.11 T [13]. This finding indicated that addition of pure Mg helps to stabilize flux motion and prevent local critical state avalanche [13].

In the power applications of a superconductor, multifilamentary wires or tapes are required, in which superconducting filaments are embedded in a matrix of a normal metal. The normal metal matrix provides protection against magnetic flux jumps and thermal quenching, as well as improves the strength to withstand the fabrication process. It is clear that the MgB₂/Mg nano-composites that we studied has many technical merits of a practical superconducting multifilamentary wire.

REFERENCES

- [1] J. Nagamatsu, N. Nakagawa, T. Muranaka, Y. Zenitani, and J. Akimitsu, "Superconductivity at 39 K in magnesium diboride," *Nature*, vol. 410, pp. 63–64, Mar. 2001.
- [2] W. N. Kang, H.-J. Kim, E.-M. Choi, C. U. Jung, and S.-I. Lee, "MgB₂ superconducting thin films with a transition temperature of 39 Kelvin," *Science*, vol. 292, pp. 1521–1523, Apr. 2001.
- [3] C. B. Eom *et al.*, "High critical current density and enhanced irreversibility field in superconducting MgB₂ thin films," *Nature*, vol. 411, pp. 558–560, May 2001.
- [4] S. Jin, H. Mavoori, C. Bower, and R. B. van Dover, "High critical currents in iron-clad superconducting MgB₂ wires," *Nature*, vol. 411, pp. 563–565, May 2001.
- [5] Q. Li and G. Gu, to be published.
- [6] A. A. Polyanskii, X. Y. Cai, D. M. Feldmann, and D. C. Larbalestier, *Nano-Crystalline and Thin Film Magnetic Oxides*. Dordrecht: Kluwer, 1999, pp. 353–370.
- [7] Y. Zhu, A. R. Moodenbaugh, G. Schneider, J. W. Davenport, T. Vogt, Q. Li, G. Gu, D. A. Fischer, and J. Taftø, "Unraveling the symmetry of the hole states near the Fermi level in the MgB₂ superconductor," *Phys. Rev. Lett.*, vol. 88, p. 247 002, Jun. 2002.
- [8] Y. Zhu, L. Wu, V. Volkov, Q. Li, G. D. Gu, A. R. Moodenbaugh, M. Malac, M. Suenaga, and J. Tranquada, "Microstructure and structural defects in MgB₂ superconductor," *Physica C*, vol. 356, pp. 239–253, Nov. 2001.
- [9] Q. Li, Y. N. Tsay, M. Suenaga, R. A. Klemm, G. D. Gu, and N. Koshizuka, "Bi₂Sr₂CaCu₂O_{8+δ} Bicrystal *c*-axis twist Josephson junctions: A new phase-sensitive test of order parameter symmetry," *Phys. Rev. Lett.*, vol. 83, pp. 4160–4163, Nov. 1999.
- [10] Q. Li, Y. N. Tsay, Y. Zhu, M. Suenaga, G. D. Gu, and N. Koshizuka, "Electromagnetic properties of high angle [001] twist grain boundaries in Bi₂Sr₂CaCu₂O_{8+δ} bicrystals," *IEEE Trans. on Appl. Superconductivity*, vol. 7, pp. 1584–1587, June 1997.
- [11] Q. Li, Y. N. Tsay, M. Suenaga, G. Wirth, G. D. Gu, and N. Koshizuka, "Superconducting transport properties of 2.2-GeV Au-ion irradiated *c*-axis twist Bi₂Sr₂CaCu₂O_{8+δ} bicrystals," *Appl. Phys. Lett.*, vol. 74, pp. 1323–1325, Mar. 1999.
- [12] D. C. Larbalestier *et al.*, "Strongly linked current flow in polycrystalline forms of the superconductor MgB₂," *Nature*, vol. 410, pp. 186–189, Mar. 2001.
- [13] Z. Ye, Q. Li, G. D. Gu, J. J. Tu, W. N. Kang, E.-M. Choi, H.-J. Kim, and S.-I. Lee, "Magneto-optical studies of critical states in *c*-axis oriented MgB₂ thin film and bulk MgB₂/Mg nano-composites," *IEEE Trans. on Appl. Superconductivity*, submitted for publication.